A Study on Deformation Characteristics of the Plane Strain Punch Stretching Test

Youngsuk Kim* and Dongwon Jung**

(*Received July 21, 1997*)

Recently, a new simple test method called plane strain stretching (PSS) test has been developed to evaluate the stamping formability of sheet materials. From the previous studies, the PSS test has been proved to have a good reproducibility and to show good correlation with the press performance. In order to clarify the deformation characteristic of the PSS test and to investigate the effect of material and process variables on the performance of the PSS test, 3-dimensional finite element simulations for the PSS test were performed and its results are compared with those of experiments.

Key Words: Stamping Formability, Sheet Material, Plane Strain Punch Stretching Test, Finite Element Simulation

1. Introduction

The stamping process plays an important role in the automotive industry. Various deformation modes such as stretching, drawing, bending, or a combination of these occur during the stamping process. Currently, there are several kinds of experimental and simulative tests that duplicate well each deformation mode occurring in the stamping process, as discussed in (Ghosh. et. al., 1984). Among these simulative tests, the Erichsen cup test, Swift cup drawing test, and the hemispherical punch stretching test (LDH report, 1990) are frequently used to evaluate the material formability. However, these test methods sometimes produce poor data reproducibility and unrealistic evaluation, especially for the zinc-coated steel sheets which are widely used in car bodies for their excellent anticorrosion property. In order to successfully obtain the desired shape of a panel, it is necessary to avoid forming failures such as local necking and shape inaccuracy and to assure the stamping formability of sheet material.

* Department of Mechanical Engineering, Kyungpook National University.

** Department of Mechanical Engineering, Jaeju National University.

Recently, two simple and effective test methods have been developed to evaluate the stamping formability of sheet materials. One is the new Ohio State University Formability test (Saunders and Wagoner, 1993 ; Suh and Wagoner) and the other is the Kim's plane strain stretching test (Kim, et al., 1993 ; Kim and Park, 1994a ; Kim and Park 1994b). In the OSU formability test a long rectangular specimen is uniformly stretched under the action of a long, small radius of cylinderical punch until the failure of the specimen occurs in plane strain deformation mode. Some finite element simulations were performed to investigate the effect of the tool geometry and the specimen size on the deformation characteristic. Therein, the optimum condition of these parameters is ascertained (Saunders and Wagoner, 1993 ; Suh and Wagoner, 1993).

However, in the PSS test, a specially designed cylindrical punch is used to assure a plane strain stretching deformation at overall area of the rectangular specimen with a proper width. In the PSS test the specimen width of 126mm, critical width, for punch geometry of 70mm in width and 70mm in length with punch corner radius of 5mm yields a plane strain deformation of the specimen for various automotive sheet materials including high strength steel sheet and aluminum sheet

(Kim, et al., 1993). The limiting punch height (LPH) value measured at plane strain fracture is used as a measure of material formability. The PSS test showed good reproducibility for various automotive sheet materials and good correlation with press performances.

The characteristic of the PSS test can be clarified by investigating the effect of the material and process variables on the results of the PSS test. However, due to the limitation on the arbitrary assignment of the material and process variables in the real experiments the numerical virtual test with properly designed variables should be frequently referred. The finite element method (FEM) with robust calculation procedures and extensive verification of the results could be suited for this purpose (Saunders and Wagoner, 1993 ; Suh and Wagoner, 1993 ; Park and Lee, 1994 ; Yoshida et al., 1993). Due to significant advances in the simulation of sheet metal forming processes using FEM it is now possible to make realistic analyses of sheet metal forming operations that taking the material and process variables into account.

In this paper, the detailed characteristics of the PSS test are studied by using the commercially available 3-dimensional stamping simulation FEM code, namely the explicit dynamic code PAM-STAMP version 2.1 (PAM-STAMP, 1992). The effect of material variables (material anisotropy parameter and work hardening exponent) and process variables (specimen width and coefficient of friction) on the strain distributions and the LPH values would be simulated, and then the numerical results will be compared with experimental ones.

2. Finite Element Simulation with PAM-STAMP

2.1 Finite element modelling

Figure 1(a) and (b) show schematics of tool set up geometry -punch, blank holder and die- under testing and tested specimen of PSS test, respectively.

Figure 2(a) and (b) show the finite element model for the PSS test process and the schematic

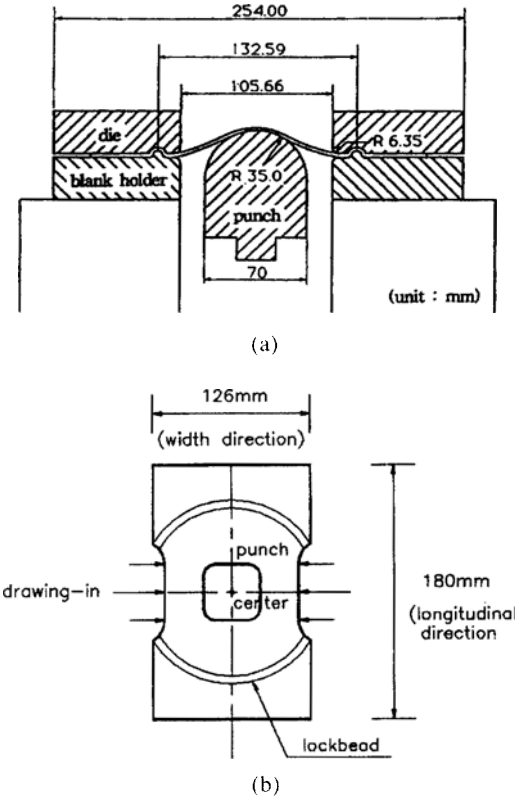

Fig. 1 Schematics of (a) tool set up geometries and (b) the tested specimen of plane strain punch stretching test.

view of the deformed/undeformed specimen, respectively. Due to the symmetry of deformation, FE simulation was done for one quarter of the specimen. The uniform mesh of 2400 quadrilateral shell elements (40 elements in width direction and 60 elements in longitudinal direction) with 3 integration points were used in the FE simulations. The average element size is about 1.5mm in width and 1.5mm in length throughout this work. In the Fig. 2(b) the numbers 1, ···, 4, ···, 7 along the longitudinal direction of the specimen denotes the area where the strain was measured. These areas are located at intervals of 7.5mm from the center in the undeformed specimen.

2.2 Material properties

Four materials including high strength steel and austenitic stainless steel were tested in this study. Table 1 shows the mechanical properties of

the tested materials and LPH values measured at PSS test. Tensile tests were performed at a con stant straining speed of 10mm/min with ASTM E-8 standard tensile specimens. All values in the table are the weighted averages of the values of 0°, 45°, and 90° with respect to the rolling direction. The parameters characterizing the uniaxial stress-plastic strain response of the materials used in FE calculations, are given also in the table in terms of the parameters in Krupkowsky's (or Swift's) work hardening law and are expressed as

$$\sigma = K(\varepsilon_0 + \varepsilon)^n \quad (1)$$

where K is the work hardening coefficient and n is the work hardening exponent. σ, ε and ε_0 is the equivalent stress, equivalent strain and offset strain, respectively.

The property of plastic anisotropy of the material is assumed to be expressed by the following Hill's anisotropy theory for the case of normal anisotropy

$$\sigma_x^2 + \sigma_y^2 - \frac{2R_n}{(1+R_n)}\sigma_x\sigma_y = \sigma_{yp}^2 \quad (2)$$

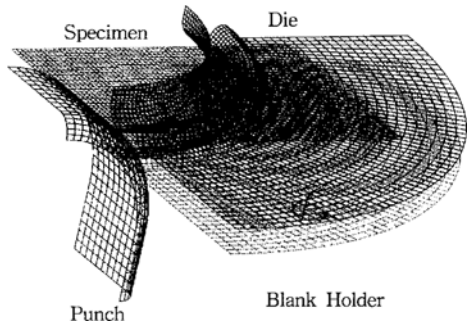

(a)

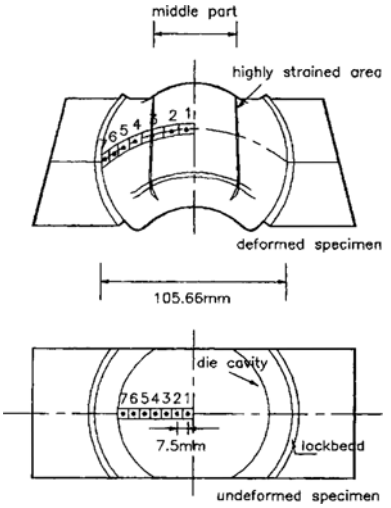

(b)

Fig. 2 Finite element model of the PSS test process (a) and schematic view of the deformed specimen with the 1, ···, 4, ···, 7 numbers denoting the strain measured element (b).

Table 1 Mechanical properties of tested materials.

Material	t (mm)	YP (MPa)	TS (MPa)	El (%)	r 15%	n 10%-20%	K (MPa)	ε_0	$LPH_{(exp.)}$ (mm)
CQ	0.79	186	315	48.2	1.59	0.23	527	0.0035	33.4
DDQ	0.78	184	285	49.4	1.72	0.24	527	0.0052	34.1
H135R	0.75	224	348	38.8	1.52	0.22	610	0.0032	30.0
SUS304	0.78	325	520	50.6	0.72	0.41	1205	0.0027	37.8

* Tensile specimen : ASTM E-8 standard, t : Thickness,
E : Young's modulus, YS : Yield strength, TS : Tensile strength,
El : Total elongation, n : Work hardening exponent, K : Strength coefficient,
R_n : Normal anisotropy parameter, ε_0 : offset strain,
$LPH_{(exp.)}$: Limiting punch height measured at experiment,
CQ : Steel sheet for commercial quality
DDQ : Steel sheet for deep drawing quality
HI35R : High strength steel sheet with tensile strength of 35 kgf/mm^2 (343 MPa)
SUS304 : Austenitic (18Cr-8Ni) stainless steel

where the normal anisotropy parameter R_n is the mean Lankford value given by $(R_0+2R_{45}+R_{90})/4$ and σ_{yp} is the yield stress obtained from the tensile test.

2.3 Friction modelling

The friction behaviors of the specimen-die/specimen-holder interface and the specimen-punch interfaces are modelled by the Coulomb friction law. The coefficients of friction μ_d of the tested materials at the specimen-die/specimen-holder interface are measured by the automatic draw bead tester(Kim and Park, 1994a), which was designed to simulate the friction state of the specimen under drawing deformation mode. The tested results showed the coefficients of friction μ_d at the specimen-die/specimen-holder interface were in the range of $\mu_d=0.14\sim0.18$ for a dry specimen. However, the coefficient of friction μ_p at the specimen-punch interface could not be measured due to its stretching mode, and thus $\mu_p=0.30$ is assumed as used in the literature of FEM simulation for OSU formability test(Saunders and Wagoner, 1993).

2.4 Simulation procedures

The PSS test is performed in two steps. In the first step, the rectangular specimen with a length of 180mm and a constant width is placed between the lower blank holder and the upper die. A lockbead in circumferential direction and a high clamping force of 298. 9kN on the lockbead is applied to guarantee the pure stretching deformation without drawing the specimen into the die cavity. In the second step, the specially designed cylindrical punch moves in the vertical direction at a constant speed to deform the specimen in plane strain stretching mode until the fracture of the specimen occurs. Therefore, the FE simulation procedure also follows this test procedure. Without any statement in the following content, the friction coefficient values of $\mu_p=0.30$ and $\mu_d=0.18$ are used in the FEM simulations and the effect of material properties was evaluated for the specimen width of 126mm.

3. Results and Discussion

Figure 3(a) and (b) show the deformed shapes and the major strain distributions for the DDQ material at punch height of h=24mm and 34. 5mm, respectively. According to punch penetration, the specimen deforms naturally to wrap the radius of the cylindrical punch corner and thus the plane strain stretching deformation prevails due to no lateral draw-in from the folded flange area. As the punch height increases, the deformation of the specimen becomes localized into a narrow region as shown in Fig. 3(b), which is corresponding to the outer boundary of the contact area of cylindrical punch and specimen.

Figure 4(a) and (b) show the comparision of calculation and experiment for the major and minor strain distributions and the strain path for the highly strained element of the DDQ material with a speamen of w=126mm. The strain was measured by the Circle Grid Analyzer (CGA) after a specimen etched with 2.54mm circles was tested. From these Figures it is clear that the calculated strains along the logitudinal direction show a good agreement with the experimental

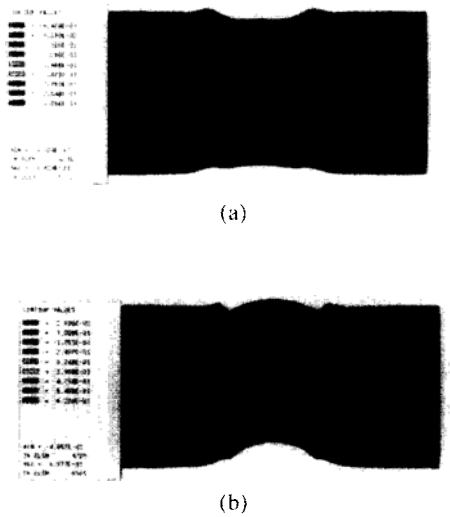

(a)

(b)

Fig. 3 Deformed shapes and major strain distributions for the DDQ material with specimen width of 126mm at punch height of (a) h=24mm and (b) h=34.5mm.

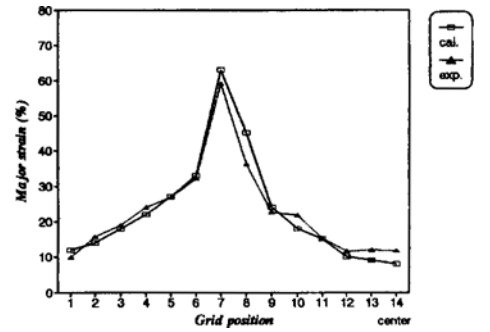

(a)

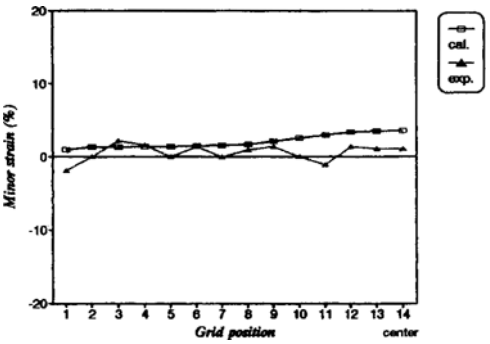

(b)

Fig. 4 Comparision of calculation and experiment for the major and minor strain distributions (a) and the strain path at the highly strained element (b) for the DDQ material of w=126mm.

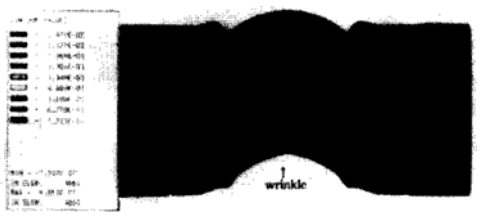

(a)

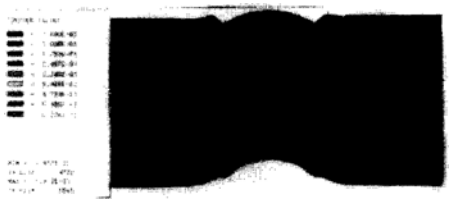

(b)

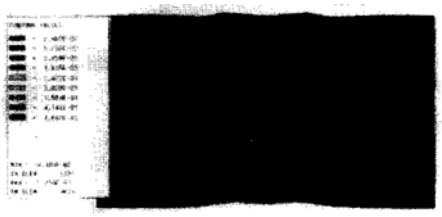

(c)

Fig. 5 Deformed shapes of the specimen of DDQ materials with three different widths of (a) w=117mm, (b) w=126mm, and (c) w=130mm for punch height h=35mm, 34mm, and 21.8mm respectively.

ones. Moreover, the strain state almost preserves almost the plane strain stretching deformation within the range of $0<e_2$(minor strain)$<2\%$ From Fig. 4(b) the strain path of the highly strained element can be said to be nearly proportional. This means that the PSS test is very valuable in evaluation of the intrinsic material formability to be tested under proportional loading.

Figure 5(a), (b) and (c) show the deformed shapes of the specimen of DDQ materials with three different widths of w=117mm, 126mm, and 130mm for punch heights of h=35mm, 34mm, and 21.8mm, respectively. This different punch height almost corresponds to the punch height at failure. In the case of the specimen width of 117mm, some wrinkles are shown at the side edge of the formed part due to some lateral draw-in. As the lateral draw-in gives the minor strain of the specimen a large negative value, it is impossible to assure a plane strain deformation in the case of the specimen with w=117mm. As the specimen width becomes narrower the lateral draw-in becomes larger so that the deformation of the specimen deviates gradually away from the plane strain deformation ($\varepsilon_1>0$, $\varepsilon_2=0$) to draw ing deformation ($\varepsilon_1>0$, $\varepsilon_2<0$). This lateral draw-in for the case of w=117mm gives a higher LPH value than that for w=126mm. On the other hand, a negligible lateral draw-in is shown at w =130mm and the specimen exhibits a corner fracture at the radius of the punch corner. This fracture mode for w=130mm is due to local large stretch bending deformation exceeding the material's capacity for stretching deformation and is

responsible for drastically lowering the punch height value measured at fracture as discussed in Kim and Park (1946b). Therefore, it can be said that the calculated deformation behaviors well simulate the deformation phenomena observed in experiments and also the predicted fracture locations agree with the experimental ones such as Fig. 2 in Ref. 7.

Figure 6 shows the deformed shapes and the major strain distributions for the specimen of HI35R material at h=30mm in PSS test simulation with w=126mm. The middle part between the left and right side of the highly strained area is responsible for uniform stretching deformation. Therefore, the uniform stretchability of the specimen may depend on the magnitude of the area of the middle part. Compared with Fig. 3(b) of DDQ material, in the case of HI35R material, the highly strained area moves to the center of the specimen and thus the area of the middle part become smaller, more precisely 42mm in HI35R material and 48mm in DDQ material at the original element position. Therefore, it can be expected that the HI35R material would show a lower LPH value than that in case of DDQ material.

Figure 7(a) and (b) show curves of thickness variation versus punch stroke for the 5 elements marked as A, B, C, D, E around the highly strained area for DDQ and HI35R materials, respectively. The A and B elements are located just below the highly strained D element. Also, the C and E elements are located just above the D element. Generally, as the punch stroke increases, the thickness of the elements, near the highly strained area, decreases rapidly due to stretching deformation. However, after failure occurred the stress acted on the area is released, thus there is no more thinning of these elements. The point indicating a drastic change of thickness variation corresponds to the calculated LPH value (LPH_{cal}) in FE simulation. In the case of DDQ material, the LPH_{cal} value is approximately 34.0mm which agrees with the experimental result of LPH_{exp}= 34.1mm.

From the comparison of Fig. 7(a) and (b), the difference of the plane strain fracture mode for both materials may be clarified. The plane strain fracture of DDQ material having sufficient ductil-

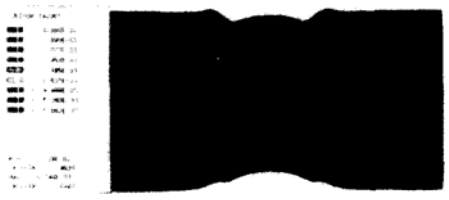

Fig. 6 Deformed shapes and the major strain distributions for the specimen of HI35R material at h=30mm with w=126mm.

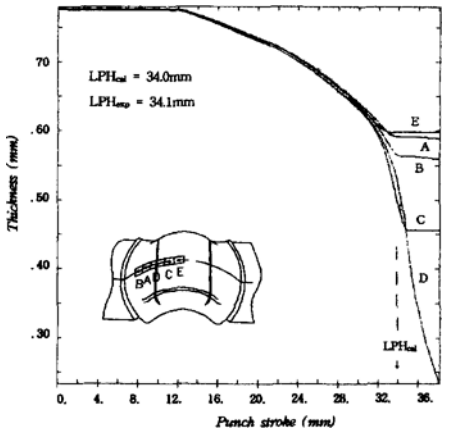

(a)

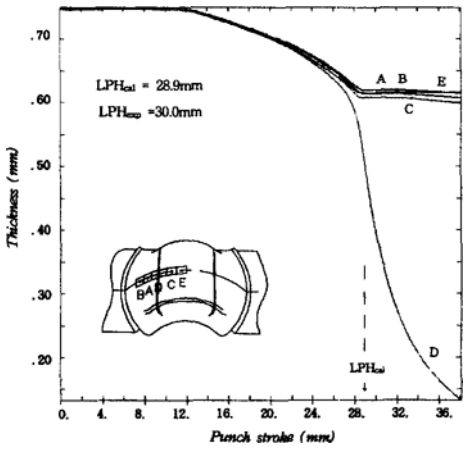

(b)

Fig. 7 Curves of thickness variation of the 5 elements around the highly strained area versus punch stroke for (a) DDQ and (b) HI35R materials.

ity proceeds with development of large plastic deformation of the uniform and local necking at elements near the highly strained area. However, in the case of HI35R material, the plane strain fracture occurs drastically without sufficient plastic deformation and necking at elements near highly strained area.

Figure 8 shows the calculated punch heights at fracture and its comparison with those of experiments for three different widths of w=117mm, 126mm and 130mm. From the Figure it is clear that the FE prediction for LPH value agrees with the experimental results. As the specimen width increases, the punch height at fracture decreases gradually. However, the punch height for the specimen of 130mm width drops drastically due to a corner fracture which occured at the radius of the punch corner as discussed in Fig. 5.

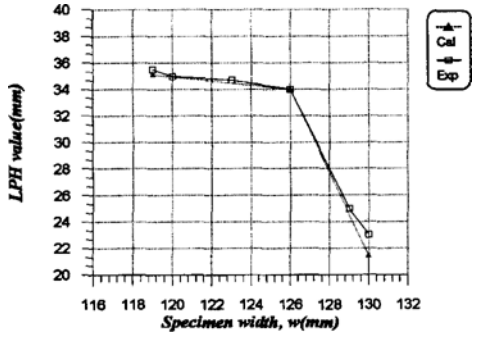

Fig. 8 Calculated punch heights at fracture and its comparison with experiments for three different widths of w=117mm, 126mm and 130mm.

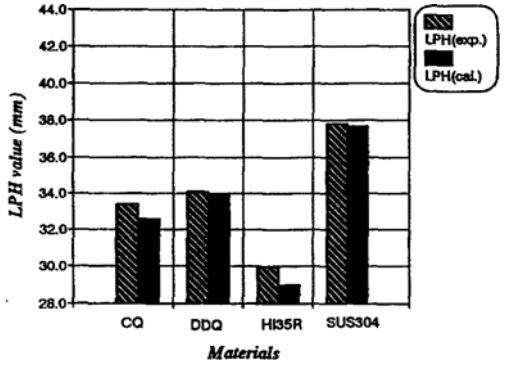

Fig. 9 Comparison between experimental LPH values (LPH_{exp}) and calculated LPH values (LPH_{cal}) in FE simulations for various materials.

Figure 9 shows the comparison between experimental LPH values (LPH_{exp}) and calculated LPH_{cal} values in FE simulations for various materials. From the Figure, it is shown that the LPH value of the PSS test ranks the material formability well as expected from the mechanical properties in Table 1. Among the tested materials, SUS304 shows a high LPH value as compared with other materials. This is due to the high value of work hardening exponent n which is responsible for uniform stretchability. However, HI35R shows poor material formability due to its poor mechanical properties such as low value of total elongation. The calculated LPH_{cal} values are estimated slightly lower than the experimental ones. However, the FE prediction of the LPH value is in agreement with the experimental results. The difference between predictions and experiments for LPH values may be reduced by introducing more realistic friction data and accurate description of the uniaxial stress-plastic strain relation for the tested material.

Figure 10 shows the effect of the coefficient of friction μ_p on LPH_{cal} value for w=126mm. The coefficient of friction was chosen to cover a realistic range of 0.05 to 0.30. As shown in the Figure, decreasing the coefficient of friction of the sheet material clearly increases the LPH value because decreasing it distributes the strain at the punch contact region more uniformly and thus lowers the strain localization.

Figure 11 shows the effect of μ_p on the strain

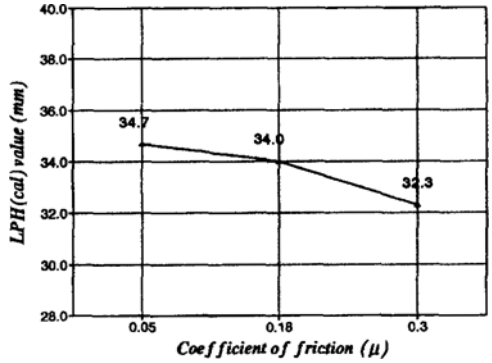

Fig. 10 Effect of coefficient of friction μ_p on LPH_{cal} value for w=126mm.

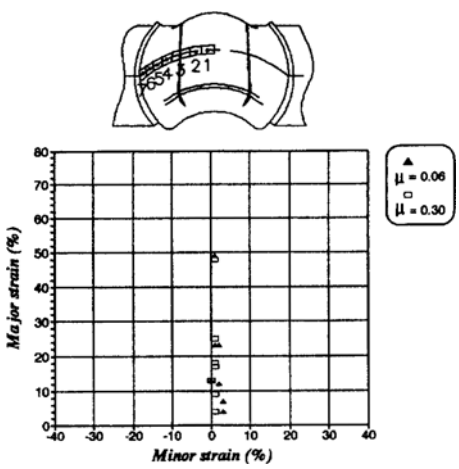

Fig. 11 Effect of μ_p on the strain distributions calculated at the elements indicated in Figure 2 (b).

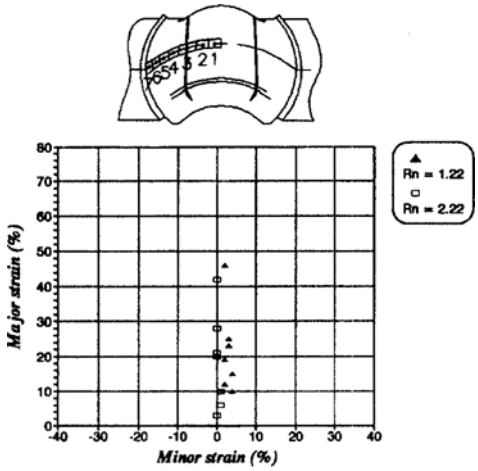

Fig. 13 Effect of R_n-value on the strain distributions calculated at the elements indicated in Figure 2(b).

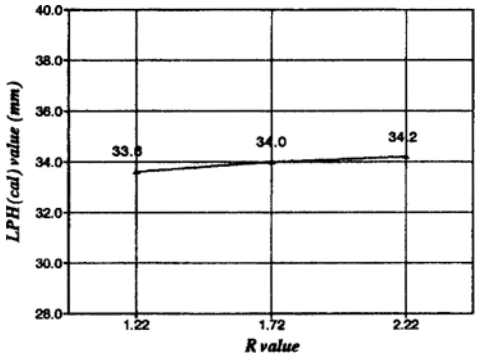

Fig. 12 Effect of normal anisotropy parameter R_n-value on LPH_{cal} value for w=126mm.

distributions calculated at the elements indicated in Fig. 2(b). As indicated in the figure, the difference of the strain distributions for two different friction conditions of $\mu_p=0.06$ and $\mu_p=0.30$ is nearly negligible. The strain distributions for both cases are nearly a plane strain state. Here, the range of the minor strain is $0\%<e_2<3\%$ for $\mu_p=0.06$ and $0\%<e_2<1\%$ for $\mu_p=0.30$. This small difference in the strain distribution of the specimen, in spite of the large difference of the friction coefficient, is due to the characteristic of the PSS test.

Figure 12 shows the effect of normal anisotropy parameter R_n-value on LPH_{cal} value for w=126mm. The effect of R_n-value on LPH_{cal} value is not so remarkable in comparison with the effect of coefficient of friction μ_p on LPH value. The reason is that in the PSS test the specimen is almost under a plane strain deformation and thus, from the plasticity theory for plane strain deformation, the LPH value does not depend on R_n-value.

Figure 13 shows the effect of R_n-value on the strain distributions calculated at the elements indicated in Fig. 2(b). As in the case of μ_p in Fig. 11, the difference of the strain distributions for different R_n-value is nearly negligible, as indicated in the Figure where the minor strain is under $0\%<e_2<4\%$ for $R_n=1.22$ and $0\%<e_2<1\%$ for $R_n=2.22$.

From the above discussion it can be concluded that the PSS test is a robust testing method for evaluating a stamping formability, as it is not so critically affected by the friction condition and the plastic anisotropy of the material.

4. Concluding Remarks

In this study, the characteristic of the plane strain punch stretching test, Kim's PSS test, was investigated by numerical and experimental methods. The Finite Element simulations using the commercially available code(PAM-STAMP) were performed to investigate the effect of mate-

rial variables and process variables on the performance of the PSS test. From the comparision of the FE simulation results and the experimental ones, it is shown that the predictions of the specimen's deformation characteristics and LPH values in FE simulations are in agreement with the experimental results. Due to its utilization of the specially designed punch shape, the PSS test could be described as a robust test method insensitive to the friction condition and the plastic anisotropy of the material.

Acknowledgements

Finacial supports of POSCO and Hyundai Motor Company are gratefully acknowledged. The authors express their thanks to Dr. Sooshik Han for valuable comments and to Mr. Hongho Ha, graduate student at Kyungpook National University, for his performing the PSS simulation.

References

Ghosh, A. K., Hecker, S. S., and Keeler, S. P., 1984 "Sheet Metal Forming and Testing, Workability Testing Techniques," G. E. Dieter ed., pp. 125~195. ASM, Metals Parks, OH.

Kim, Y. S., Park, K. C., and Nam, J. B., 1993 "Development of Plane Strain Punch Stretching test," *J. Korean Soc. Mech Engng*, Vol. 7-5, pp. 1132~1137.(in Korea)

Kim, Y. S., and Park, K. C., 1994 "Comparison of Friction Coefficients of Sheet Materials in Various Deformation Modes," *J. Korean Soc. Tech. Plasticity*, Vol. 3-1, pp. 51~62.(in Korea)

Kim, Y. S., and Park, K. C., 1994 "A Plane Strain Punch Stretching Test for Evaluating Stamping Formability of Steel Sheets," *Metal. Trans.*, Vol. 25A~10, pp. 2199~2205.

LDH Committee/NADDRG 1990 Final Report of the LDH Committee, May.

PAM-STAMP™ version 2.1, 1992 User's Manual, Pam System International, ESI-GROUP Software Product Company.

Park, C. D., and Lee, J. H., 1994 "The Development and Application of Sheet Metal Forming Technology," *Proc. Korean Soc. Tech. Plasticity Autumn Annual Conf.*, pp. 147~162.(in Korea)

Saunders, F. I., and Wagoner, R. H., 1993 "Finite Element Modelling of a New Formability Test," *Computer Application in Shaping & Forming of Materials*, Edited by Demeri, M. Y., TMS, Pennsylvania, pp. 205~220.

Suh, Y. S., and Wagoner, R. H., 1993 "Optimized Design of Tooling of the New Formability Test," Computer Application in shaping & Forming of Materials, Edited by Demeri, M. Y., TMS, Pennsylvania, pp. 221~228.

Yoshida, T, and Katayama, T, and Usuda, M, 1993 "Forming Limit Analysis of Hemispherical Punch Stretching Using Three-Dimensional Finite Element Method," *Proc. 2nd Int. Conf.* NUMISHEET'93, pp. 219~228.